International Journal of Physical Sciences Vol. 3 (12), pp. 314-320, December, 2008
Available online at http://www.academicjournals.org/IJPS
ISSN 1992 - 1950 © 2008 Academic Journals

Full Length Research Paper

Numerical simulation of a one-dimensional shock tube problem at supercritical fluid conditions

Hatem Ksibi and Ali Ben Moussa

Sfax University, IPEIS P. Box 805 Sfax 3018, Tunisia, CFDTP, ENIS, P. Box W, 3038 Sfax, Tunisia.

Accepted 17 July, 2007

The numerical computation of supercritical fluid flows is extremely challenging because of the complexity of the physical processes and the disparity of the space and time scales involved. Supercritical fluids exhibit large density fluctuations especially very close to the critical region. In this region, the perfect gas law is no longer valid and has to be replaced by a specific equation of state (EoS) as, for instance, the Altunin and Gadetskii EoS. In the present work, the problem of choosing a suitable numerical scheme for dense gas flow computations in a shock tube is addressed. In particular, the extension of the classical Roe's scheme to real gas flows is used and its performance is evaluated by comparing with the analytical profile of the dimensionless density obtained by Sod in the shock tube problem. The application of this numerical implementation near the critical region of the fluid gives significant differences compared to gas dynamics and shows a relevant behaviour of the compressibility variation and localises an important gradient of temperature in the shock tube.

Key words: Hydrodynamics, shock tube, numerical simulation, real gas flow, critical region.

INTRODUCTION

A supercritical fluid (SCF) may be defined as a substance for which both temperature and pressure are above the critical values. When a liquid is heated above its critical temperature at pressures greater than (or exceeded) the critical pressure, the transition from liquid to supercritical fluid is continuous. Close to the critical density, SCFs display properties that are to some extent intermediate between those of a liquid and a gas. For instance, a SCF may be relatively dense and dissolve certain solids while being miscible with permanent gases and exhibiting high diffusivity and low viscosity. In this phase domain, the thermal and mechanical disturbances are strongly coupled. This specific behaviour of the supercritical fluids is of particular interest both from the theoretical point of view and for many industrial applications, such as the production of nanoparticles for medical use and the extraction of chemical compounds.

A shock tube conventionally takes the form of a strong smooth wall steel pipe, of either circular or rectangular cross-section, divided into two compartments initially at different pressure values and separated by a diaphragm, see Figure 1. If we suppose that the viscous effects are negligible along the tube and we assume that the tube is sufficiently long enough to avoid reflections at the tube ends, the exact solution of the Euler equations can be obtained on the basis of a simple wave analysis. At the bursting of the diaphragm, the discontinuity between the two initial states breaks into leftward and rightward moving waves, separated by uniform solutions: a shock wave (S) followed by a contact discontinuity (C) moves to the low pressure region and rarefaction waves (R) move to the high pressure side (Sod, 1978).

In the experimental studies, shock tubes conven-tionally feature a test-section, often equipped with obser-vation windows, in which a shock process, interaction, or other phenomena are studied using specific diagnostic instrumentation such as high-speed recording techni-ques, photography, etc…. Many shock tubes used in research studies follow the conventional simple design with lengths of typically a few metres and operating with compressed air pressures up to several atmospheres.

From a numerical point of view, the shock-tube problem is a very interesting test case because the exact time-dependent solution is analytically known and can be compared with the computed solution by applying numerical approximations, (Arina, 2004; Guardone and Vigevano,

*Corresponding author. E-mail: hatemksibi@yahoo.fr.

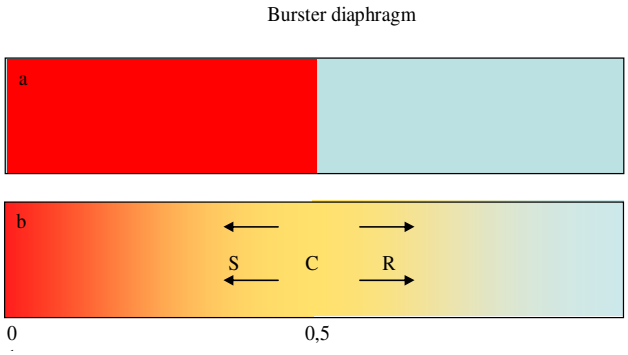

Figure1 - Shock tube at initial state (a: t= 0. s; b: t >0 s).

2004). The initial configuration of the shock-tube problem is composed by two uniform states at the same temperature but at different pressure values, separated by a discontinuity which is usually located at the middle of the tube. This particular initial value problem is known as the Riemann problem.

In this work we propose a numerical approach, based on the Roe averaged technique (Roe, 1981) written for real gas using the full EoS of Alunin and Gadestkii (1971) which is available also in the critical region. This approach, mainly following the Harten et al. (1986) and Montagné et al. (1987) algorithms, allows computing the distribution along the tube of the thermodynamics quantities at subcritical, critical or supercritical initial conditions. Here the high order of the numerical resolution is associated to the non linearity of the EoS where thermodynamic variables are calculated through a prediction-correction technique. Numerical validation is firstly reached by comparing our results with the Sod's shock tube analytical solution (1978) of a perfect gas dynamic due to a pressure falling from 1 to 0.1 bar (Sod, 1978; Toro, 2005).

Governing equations

Conservation law approximations

Considering a non viscous flow in a tube having a constant section and assuming a one dimensional problem, the system of equations can be written as:

$$\frac{\partial \mathrm{U}}{\partial \mathrm{t}}+\frac{\partial f\left(\mathrm{U}\right)}{\partial \mathrm{x}}=0$$

. !

Where $U=(\rho,\rho u,\rho E)^T$ is the vector of the conservative variables, $f=(\rho u,\rho u^2+P,\rho uE+uP)^T$ the Euler flux vector. *t* and *x* stand for the time and space coordinates. $\rho$is the density, *u* the velocity, *E* the total energy per unit of mass and P is the static pressure. By introducing the jacobian matrix of the Euler flux $\mathrm{A}(\mathrm{U})=\frac{\partial f(\mathrm{U})}{\partial \mathrm{U}}$, the system of equations can be written, in semi-conservative form, following:

$$\frac{\partial \mathrm{U}}{\partial \mathrm{t}}+\mathrm{A}(\mathrm{U})\frac{\partial \mathrm{U}}{\partial \mathrm{x}}=0 \qquad (2)$$

The numerical procedure is based on an approximate Riemann solver, following the Roe technique that needs to know an averaged state between the states U_L and U_R of the Riemann problem at the grid interfaces:

$$\boldsymbol{f}(\boldsymbol{U_R})-\boldsymbol{f}(\boldsymbol{U_L})=\hat{\boldsymbol{A}}(\boldsymbol{U_L},\boldsymbol{U_R})\cdot(\boldsymbol{U_R}-\boldsymbol{U_L}) \qquad (3)$$

To ensure conservativity and consistency, the Roe matrix (Â) must be evaluated by using the Roe average quantities [4]:

The average density: $\overline{\rho}=\sqrt{\rho_R\,\rho_L}$

(4)

The average velocity $\overline{\boldsymbol{u}}=\frac{\sqrt{\rho_R}\,\boldsymbol{u}_R+\sqrt{\rho_L}\,\boldsymbol{u}_L}{\sqrt{\rho_R}+\sqrt{\rho_L}}$

(5)

And the average total enthalpy: $\overline{\boldsymbol{H}}=\frac{\sqrt{\rho_R}\,\boldsymbol{H}_R+\sqrt{\rho_L}\,\boldsymbol{H}_L}{\sqrt{\rho_R}+\sqrt{\rho_L}}$.

(6)

These averaged quantities are valid both for a perfect gas and a real fluid. The difference between these two cases lies in the calculation of the average of the speed of sound. In the case of a real fluid it is necessary to recognize special formulations of the pressure derivatives (Montagné et al., 1987).

Boundary conditions

The tube is supposed to be closed at both ends. The right and left boundaries of the computational domain are thus ideal solid walls. Since the integration time is relatively short, the shock and rarefaction waves never reach the end walls, and so, conditions at these boundaries are well known. Initially the fluid is at rest and its temperature is prescribed at T_0=305 K (T_0> T_c) in order to cover the critical region of the fluid. Pressures from both sides of the diaphragm are set at different levels. The initial values for the different test-cases can be seen in tables 1, 2 and 3.

Numerical methods

To obtain a numerical approximation of the Euler equa-

Table 1. Initial conditions of the perfect gas shock tube.

Region	Density ($kg.m^{-3}$)	Pressure (bar)	Temperature (K)	
			EoS (8)	ideal gas
Left	1.0	1.0	529.6	529.3
Right	0.125	0.1	423.55	423.45

Table 2. Initial conditions of the supercritical/subcritical shock tube

Region	Pressure (bar)	Temperature (K) From EoS (14)
Left	75.0	305
Right	65.0	305

Table 3. Initial conditions of the near critical region shock tube.

	Region	Pressure (bar)	Temperature (K) EoS (14)
Subcritical	Left	55	305
	Right	50	
Critical	Left	75	
	Right	70	
Supercritical	Left	105	
	Right	100	

equation (1), we use a numerical scheme based on Roe Riemann solver (Montagné et al., 19878]. The scheme used is based on a Finite-Volume approximation. It is of high resolution, that is, it recovers a second order accuracy away from discontinuities. It however satisfies the Harten's Total Variation Diminishing (TVD) constraints to avoid the spurious oscillation in the vicinity of the discontinuities. A stability condition is required and, assuming a constant grid size (Δx), the time step (Δt) is calculated by using:

$$\Delta t = \frac{N_{CFL}\Delta x}{\max\left(\left|\lambda_i\right|\right)}, \qquad (7)$$

Where $\max\left(\left|\lambda_i\right|\right)$ is the maximum wave speed and N_{CFL} the required Courant (CFL) number.

Equation of state

The development of equations of state (EoS) and their applications to the correlation and the prediction of phase equilibrium properties is an important field of research. The Altunin and Gadetskii EoS was given to describe the thermodynamic properties of the pure carbon dioxide. Following this specific EoS, the behaviour of supercritical, liquid or gas states of carbon dioxide are accurately fitted. As all thermodynamic properties divergence in the vicinity of the critical point (mainly the compressibility factor), the Altunin and Gadetskii EoS needs other corrective terms to more accurately fit the singular behaviour and to increase the robustness in the calculation of the thermodynamic functions as, for instance, the specific heat at constant volume, the pressure and the speed of sound.

The original equation proposed by Altunin and Gadetskii describes with a great accuracy the carbon dioxide behaviour in the regions far from the critical region. However, to supply the Altunin and Gadetskii EoS in the vicinity of the critical point, one must used a special EoS obtained by digitalizing corrective abacus given in the literature (Angus et al., 1976). This work is followed by a numerical estimation of different thermodynamic functions as C_v, in the vicinity of the critical point, using series expansion techniques (Ksibi and Moussa, 2005).

The analytic Altunin and Gadestkii EoS is written as:

$$Z = \frac{P_A}{\rho RT} = 1 + \rho_r \sum_{i=0}^{9}\sum_{j=0}^{6} b_{ij}\left(\tau - 1\right)^j\left(\rho_r - 1\right)^i \qquad (8)$$

Where $\rho_r=\rho/\rho_c$ and $\tau=T_c/T$. Z is the compressibility factor and R is the perfect gas constant. The subscript "c" indicates values at the critical point. The b_{ij} coefficients can be found in the IUPAC tables, (Angus et al., 1976). A separate EoS was needed for the critical region within about $\pm$ 5 K of the critical temperature. This equation is expressed in terms of the polar coordinates, r and θ, in the phase plane, centred on the critical point, Schofield et al (1969). The distances to the critical value for the density and the temperature are expressed following:

$$\Delta T = \frac{\left(T - T_c\right)}{T_c} = r\left(1 - b^2\theta^2\right) \qquad (9)$$

$$\Delta\rho = \frac{\left|\rho - \rho_c\right|}{\rho_c} = r^\beta g\theta \qquad (10)$$

The pressure in the vicinity of the critical point (P_S) is deduced from the previous equations by the following parametric equation:

$$\Delta P = \frac{\left|P_S - P_c\right|}{P_c} = r^{\beta(\delta+1)}q(\theta) + c\Delta T + ar^{\beta\delta}\theta\left(1 - \theta^2\right) \qquad (11)$$

Where q is a function of θ, given by:

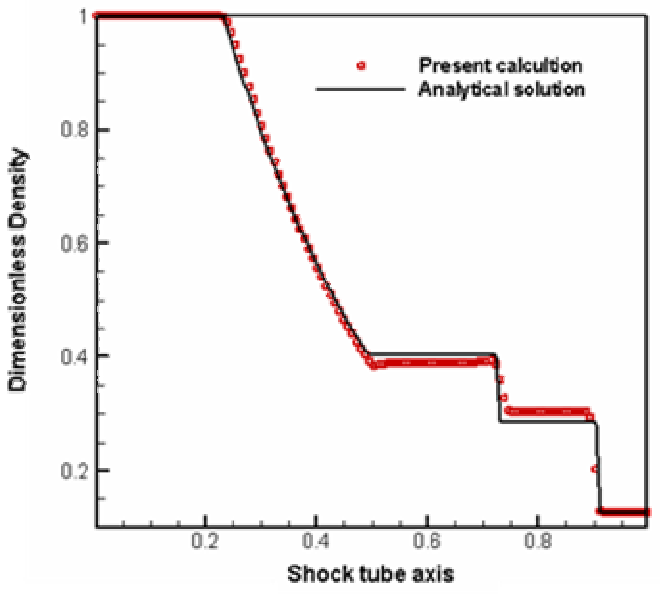

Figure 2- Numerical validation of the shock tube problem for sub-critical conditions, at a dimensionless time t = 0.2 s

$$q(\theta) = 36.98893 - 82.07960\theta^2 + 56.660530\theta^4 \qquad (12)$$

The complete EoS is obtained through the combination between equations (8) and (11) by using a switch function f(r), depending on the distance to the critical point:

$$P = f(r).P_A + [1 - f(r)]P_S \qquad (13)$$

Where f(r) is expressed by:

$$f(r) = 1 - \left[1 - e^{(-0,01/r)^{n_1}}\right].\left[1 - e^{(-0,05/r)^{n_2}}\right] \qquad (14)$$

And P_A is the analytic pressure deduced from equation (8).
Values of different constants needed to evaluate the pressure at the critical region P_S are:

n_1=3/2 ; n_2=3; a=0.065; β=0.347; δ=4.576; g=1.491, b^2=1.4402.
The value of the parameter "c" depends on the relative temperature (T/Tc); *i.e.* for T>Tc,
c= 240.435 and for T≤Tc, c= -58.383.

Numerical results and discussions:

Numerical validation

The validation of the numerical code is performed by comparing the numerical solution with the analytical one proposed by Sod and established for a perfect gas (air) flow in a shock tube. The initial conditions are summarized in table 1 where the temperature is obtained by using both the Altunin and Gadestkii and the ideal gas EoS. At the initial state, a diaphragm, located in the middle of the shock tube, separates the carbon dioxide considered as a perfect gas at two different states from both sides of the diaphragm. The density and pressure jumps are chosen so as to recover the three types of wave (shock wave "S", contact discontinuity "C", and rarefaction waves "R") in the tube.

The pressure on the left side of the diaphragm is 10 times higher than the one on the right side. At time t = 0 when the diaphragm is broken, the discontinuity between the two initial states leads to leftward and rightward moving waves, separated by uniform states. A shock wave moves to the low pressure region (toward the right side) followed by a contact discontinuity moving at the local speed of the flow. Expansion waves move to the high pressure side (toward the left side). Since the computation stops before the waves reach the end-walls of the shock tube, the boundary conditions are trivial at both ends of the shock tube. The simulations are performed by using a CFL number equal to 0.2.

In these calculations, we have used a regular grid with 100 grid-nodes. From Figure 2, we show that the present code has captured with accuracy the jumps across discontinuities. The velocities of discontinuity propagations have also been accurately computed. When the simulation is performed on the sub-critical conditions ($T > T_c$ and $\rho < \rho_c$), differences with the exact ideal gas solution are noticeable on the constant states around the contact discontinuity. We must also notice that the velocity of the contact discontinuity is slightly more important than in the case of an ideal gas. These differences are only due to the thermodynamic behaviour of the fluid within the sub-critical region (EoS (8)) which induces a higher flow velocity than the ideal gas configuration between the last expansion wave and the shock wave.

Shock tube at high pressure initial conditions

Numerical simulations are also performed by considering the carbon dioxide at supercritical state on the left side, whereas the carbon dioxide is set at subcritical conditions, on the right side (see table 2). Numerical results greatly improve the accuracy of the capture of rarefaction, contact discontinuity, and shock waves.

In Figure 3, the dimensionless density of the carbon dioxide is depicted along the tube axis at the several times. We show that at every time, S, C and R waves are well captured along the tube. During time, shock wave (S) reaches the left side tube while keeping a constant density behind the shock. The contact discontinuity is captured at the half of the tube for the different cases. At

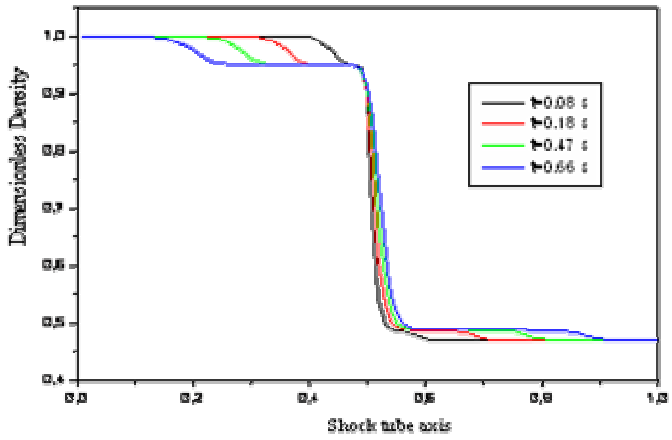

Figure 3- Dimensionless density profiles along the shock tube for different time steps.

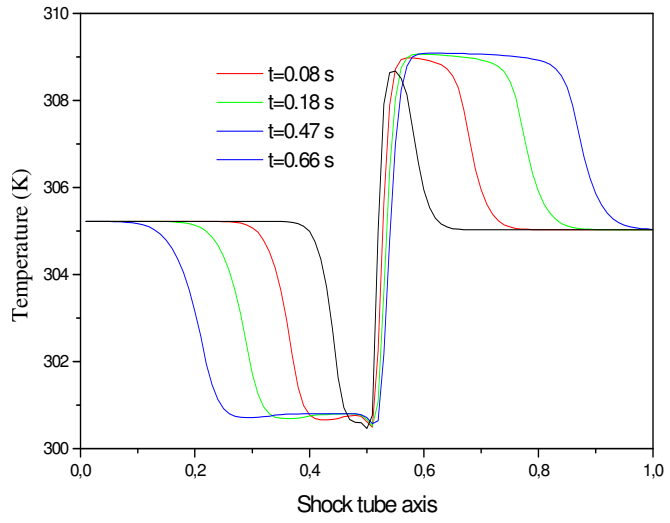

Figure 4- Temperature profiles along the shock tube for different time steps.

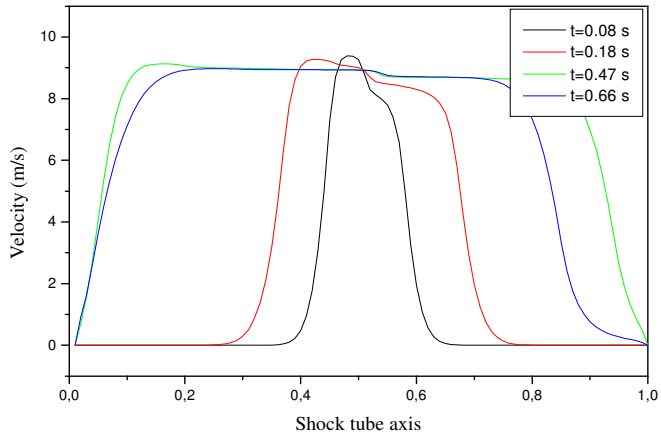

Figure 5. Velocity profiles along the shock tube for different time steps.

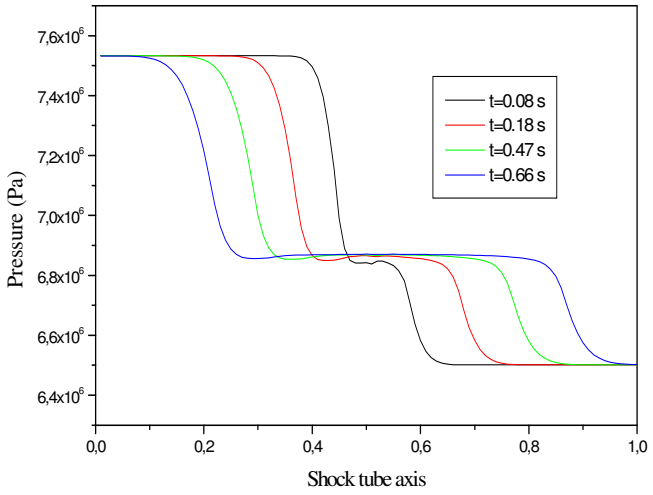

Figure 6. Pressure profiles along the shock tube for different time steps.

the other side, the rarefaction wave R reaches the right side while keeping a constant density at the right end of the tube.

The temperature evolutions are shown on figure 4. Regarding the temperature amplitudes in the shock tube, it is solicited to an important thermal gradient (about six degrees). In the left compartment, the bursting of the diaphragm involves a local expansion upstream of the wave C that generates a fall of temperature. Whereas, the contribution of the matter implies a local compression downstream of the wave C which generates an elevation of the temperature. This behaviour is supported by the hyper compressibility of the carbon dioxide in the vicinity of its critical point.

Concerning the speed profile along the tube (figure 5) the initially stagnant fluid, moves abruptly in the both sides of the tube when the diaphragm is burst. At t = 0,66s, the fluid has practically a constant speed along the tube (about 9 m/s) except at its end walls where no motion conditions are imposed, the fluid velocity exceeds

Similarly to the density profile, figure 6 shows the pressure behaviour in the tube for the different shocks waves S, C and R at different time steps. We note that the depressurisation goes proportionally to time in the left side which involves a compression of the fluid inside the right compartment.

Shock tube behaviour at critical initial conditions

In order to show the importance of the Sod problem modelling in the vicinity of the critical region, numerical implementations are selected so as to cover different regions of the phase diagram of the carbon dioxide, mainly: the subcritical zone ($T>T_C$ and $P<P_C$); the critical zone and the supercritical zone ($T>T_C$ and $P>P_C$).

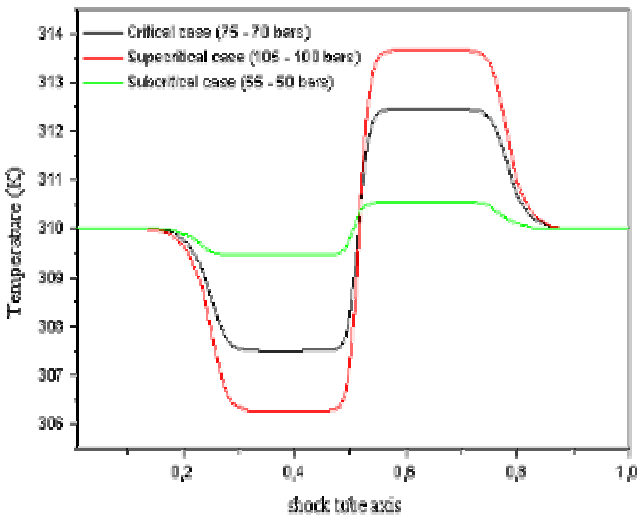

Figure 7. Temperature profiles along the shock tube for different expansion ratios (effect of the critical region behaviour).

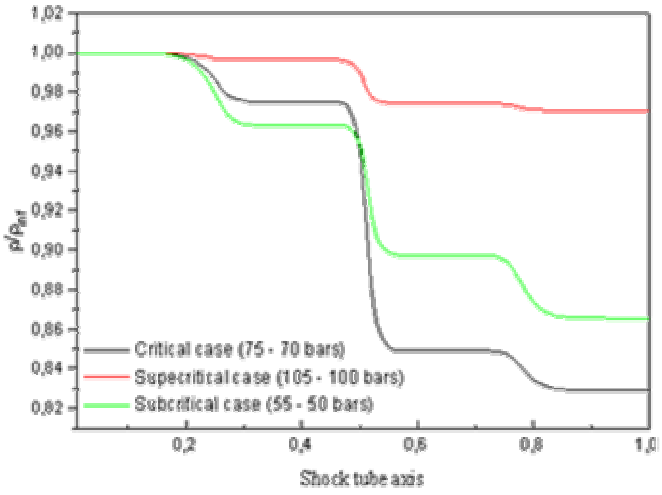

Figure 8. Dimensionless density profiles along the shock tube for different expansion ratios (effect of the critical region behaviour)

In these three test cases, the pressure jump (P_L-P_R) between the left and the right sides of the tube is kept constant and equal to 5 bars. The initial temperature is considered constant along the tube and set at 310 K.

On the Figure 7, we illustrate the profile of the temperature along the shock tube at t = 0.28 s. The temperature is maintained constant at the end-walls. We initially distinguish an anti symmetry of the temperature variation compared to the position of the diaphragm (x = 0.5). The subsonic case (expansion from 55 to 50 bars) provides a small variation in the temperature of 0.5 K. This amplitude climbs to 4 K in the supercritical case (from

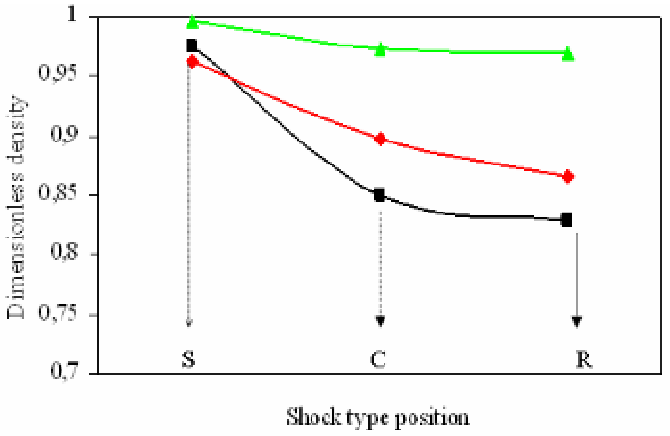

Figure 9. Density falls under the action of the various shock waves (S, C, R).

105 to 100 bars) and generates mainly a strong gradient making it possible to induce in a relevant way a thermal transfer in the shock tube.

Concerning the variation of the carbon dioxide density along the shock tube, it varies by marking the various waves C, R and S in different ways relating to the pressure level. Indeed, the variation of □ in the supercritical case (P_L=105 and P_R=100 bars) implies a fall of this one on three various levels similarly with the case of shock tube of a perfect gas, (Figure 8). Nevertheless, the state being dense like a liquid, the variation of □ remains tiny and lower than 2.5%. In the subcritical case (P_L=55 and P_R=50 bars), the density follows the same profile and locates the waves C, R and S correctly. Moreover, we notice that the dimensionless density variation becomes more amplified.

Applying a pressure level around the critical one (P_c= 73.8 bars), the variation of the density appears exactly as the last two cases but a significant decrease of the density is reached (about 20%). Here, the high compressibility of the state implies a non linearity of the density falls with the pressure level differently to the temperature oscillations as described before. Indeed, figure 9 shows this singular behaviour of the dimensionless density values across different waves in the shock tube. For the same difference in pressure (P_L - P_R), the variation of the density is very significant while passing by the critical region, compared with the subcritical and supercritical cases.

Conclusion

This paper discusses the propagation of shock waves through a shock tube containing initially supercritical fluid. It was found that the numerical calculations give similar results presented by several authors for a perfect gas. Applications of the supercritical state by using a specific

EoS, valid near and far from the critical region, in a shock tube problem give similar profiles of density, pressure and velocity to that of perfect gas. Nevertheless, computing the shock tube problem at high pressure levels shows a particular behaviour of the fluid density near the critical region and an important thermal gradient in the shock tube.

REFERENCES

Sod GA (1978). A survey of several finite difference methods for systems of nonlinear hyperbolic conservation laws. J. Computational Physics, (27): 1–31.

Arina R (2004). Numerical simulation of near-critical fluids. Applied Numerical Mathematics (51): 409–426.

Guardone A, Vigevano L (2004): Assessment of thermodynamic models for dense gas dynamics. Physics of Fluids 16, (11): 3878-3887.

Roe PL (1981). Approximate Riemann solvers, parameter vectors, and difference schemes. J. Computational Physics, 43 357–372.

Altunin W, Gadetskii OG (1971). Equation of State and Thermodynamic Properties of Liquid and Gaseous Carbon Dioxide. Teploenergetika, 18, (3): 120-125.

Yee HC, Harten A (1986). Implicit TVD Schemes for Hyperbolic Conservation Laws in Curvilinear CoordinatesAIAA J. 25: 266-274.

Toro EF (2005). Riemann Solvers and Numerical Methods for Fluid Dynamics - A Practical Introduction, XIX Edition, Springer Published,

Montagné JL, Yee HC, Harten A (1987). in: Dr Hill library (Eds), Proceedings of 7th GAMM Conference on Numerical Methods on Fluid Mechanics, Louvain la Neuve.

Angus S, Armstrong B, de Reuck KM (1976) International Thermodynamic Tables of the Fluid State Carbon Dioxide 3. IUPAC Pergamon Press, Oxford.

Ksibi H, Moussa AB (2005). Numerical implementation of the Altinun and Gadetskii EoS at the critical region og the pure carbon dioxide. Proceedings of 10th European Meeting on Supercritical Fluids**,** Reactions, Materials and Natural Products Processing, Strasbourg.

Schofield PJD (1969). Litster and J. T. Ho, Correlation between Critical Coefficients and Critical Exponents. Phys. Rev. Letters, 23: 1098-1102.